ELSEVIER

FEMS Microbiology Ecology 51 (2004) 55–70

FEMS MICROBIOLOGY Ecology

www.fems-microbiology.org

Characterization of functional bacterial groups in a hypersaline microbial mat community (Salins-de-Giraud, Camargue, France)

Aude Fourçans [a], Tirso García de Oteyza [b], Andrea Wieland [c], Antoni Solé [d], Elia Diestra [d], Judith van Bleijswijk [e], Joan O. Grimalt [b], Michael Kühl [c], Isabel Esteve [d], Gerard Muyzer [f], Pierre Caumette [a], Robert Duran [a,*]

[a] *Laboratoire d'Ecologie Moléculaire EA 3525, Université de Pau et des Pays de l'Adour, avenue de l'Université, BP 1155, F-64013 Pau Cedex, France*
[b] *Department of Environmental Chemistry (ICER-CSIC), E-08034 Barcelona, Spain*
[c] *Marine Biological Laboratory, Institute of Biology, University of Copenhagen, DK-3000 Helsingør, Denmark*
[d] *Department of Genetics and Microbiology, Autonomous University of Barcelona, E-08193 Bellaterra, Spain*
[e] *Royal Netherlands Institute of Sea Research, Texel, The Netherlands*
[f] *Department of Biotechnology, Delft University of Technology, NL-2628 BC Delft, The Netherlands*

Received 20 October 2003; received in revised form 19 April 2004; accepted 13 July 2004

First published online 20 August 2004

Abstract

A photosynthetic microbial mat was investigated in a large pond of a Mediterranean saltern (Salins-de-Giraud, Camargue, France) having water salinity from 70‰ to 150‰ (w/v). Analysis of characteristic biomarkers (e.g., major microbial fatty acids, hydrocarbons, alcohols and alkenones) revealed that cyanobacteria were the major component of the pond, in addition to diatoms and other algae. Functional bacterial groups involved in the sulfur cycle could be correlated to these biomarkers, i.e. sulfate-reducing, sulfur-oxidizing and anoxygenic phototrophic bacteria. In the first 0.5 mm of the mat, a high rate of photosynthesis showed the activity of oxygenic phototrophs in the surface layer. Ten different cyanobacterial populations were detected with confocal laser scanning microscopy: six filamentous species, with *Microcoleus chthonoplastes* and *Halomicronema excentricum* as dominant (73% of total counts); and four unicellular types affiliated to *Microcystis*, *Chroococcus*, *Gloeocapsa*, and *Synechocystis* (27% of total counts). Denaturing gradient gel electrophoresis of PCR-amplified 16S rRNA gene fragments confirmed the presence of *Microcoleus*, *Oscillatoria*, and *Leptolyngbya* strains (*Halomicronema* was not detected here) and revealed additional presence of *Phormidium*, *Pleurocapsa* and *Calotrix* types. Spectral scalar irradiance measurements did not reveal a particular zonation of cyanobacteria, purple or green bacteria in the first millimeter of the mat. Terminal-restriction fragment length polymorphism analysis of PCR-amplified 16S rRNA gene fragments of bacteria depicted the community composition and a fine-scale depth-distribution of at least five different populations of anoxygenic phototrophs and at least three types of sulfate-reducing bacteria along the microgradients of oxygen and light inside the microbial mat.

Keywords: Bacterial community composition; Biomarkers; Confocal microscopy; Microbial mat; Microsensors; Bacterial diversity

1. Introduction

Photosynthetic microbial mats develop at the water–sediment interface in shallow environments such as

* Corresponding author. Tel.: +33 5 5940 7468; fax: +33 5 5940 7494.
E-mail address: robert.duran@univ-pau.fr (R. Duran).

0168-6496/$22.00
doi:10.1016/j.femsec.2004.07.012

estuaries [1,2], sheltered sandy beaches [3,4], or hypersaline salterns [5,6]. Most of these microbial mats are formed of horizontally stratified, multicolored and cohesive thin layers of several functional groups of microorganisms, such as cyanobacteria, colorless sulfur bacteria, purple sulfur bacteria and sulfate-reducing bacteria, distributed along vertical microgradients of oxygen, sulfide and light [7,8].

Hypersaline mats from salterns represent interesting ecosystems adapted to fluctuating salinity conditions. Microbial mats existing in the most hypersaline ponds of the salterns of Salins-de-Giraud (Camargue, French Mediterranean coast) have been described in ecological and microbiological, and recently molecular studies over the last 10 years [5,9–11]. These saline ponds with water salinity between 150‰ and 300‰ (w/v) contain microbial mats similar to those previously described in other hypersaline habitats [6,12]. They are formed of an upper layer of cyanobacteria belonging to the genus *Phormidium*, covering a purple layer of phototrophic bacteria mainly composed of members of the genera *Halochromatium* [13] and *Halothiocapsa* [14], well adapted to such high salinities. Molecular studies [9] showed that the bacterial composition of these mats was more diverse than expected both in Bacterial and in Archaeal groups.

In the present study, we investigated another mat from the same salterns growing in ponds with lower salinity (70–150‰ (w/v)). This mat developed over several decades in large areas used by the Saltern Company as water reservoirs for salt production. The aim of this analysis was to characterize the composition of the functional bacterial groups developing in the Camargue microbial mat. The simultaneous use of different methods for analysis of bacterial composition and microenvironment, allowed a precise in situ analysis of the Camargue mat. In the mat, the major bacterial groups were investigated by characteristic biomarkers, confocal laser scanning microscopy (CLSM), denaturing gradient gel electrophoresis (DGGE) and terminal-restriction fragment length polymorphism (T-RFLP) analysis of PCR amplified 16S rRNA genes or functional gene fragments. In order to understand the bacterial occurrence and distribution at the microscale level, all the microbiological results were related to microenvironmental gradients determined by in situ microsensor measurements.

2. Materials and methods

2.1. Sampling site description

The sampling site was in a very large shallow pond at the saltern of Salins-de-Giraud, close to the sand barrier and the sea coast (43°27′35″ N, 04°41′28″ E, Camargue, France). This pond was used for the storage of pre-concentrated seawater. In this pond of about 10 km^2 area, the water column never exceeded 20 cm depth and its salinity ranged from 70‰ to 150‰ (w/v). The photosynthetic microbial mat covered a large proportion of this pond and also of other adjacent ponds, and was constituted of thin laminated cohesive layers. Due to its development over several decades, the mat was about 5–10 cm thick. The underlying sediment was mostly composed of a mixture of sand and clay.

2.2. Sampling procedure

All mat samples analyzed were collected in May 2000, by mean of plexiglass cores. For biomarker analysis, mat cores of 26 mm inner diamater were immediately frozen until further analysis. For confocal laser scanning microscopy, two cores (18 mm i.d.) were transferred into small plastic tubes containing 2.5% (v/v) glutaraldehyde in phosphate buffer (0.2 M, pH 7.4, adjusted to the appropriate salinity with NaCl), and stored at 4 °C until further processing. For DGGE and T-RFLP, the upper 10 mm of the mat cores (35 mm i.d.) were sliced off aseptically, transferred to sterile Petri dishes, frozen in liquid nitrogen, and then stored at −80 °C.

2.3. Microsensor measurements of O_2 and oxygenic photosynthesis profiles

Depth profiles of O_2 and gross oxygenic photosynthesis were measured in May 2000. Microsensor measurements were done in situ from a small measuring platform placed above the mat. A Clark-type O_2 microsensor [15] connected to a picoammeter (UniSense A/S, Aarhus, Denmark) was manually operated with a micromanipulator (Märzhäuser, Wetzlar, Germany) mounted on a heavy solid stand. Microsensor signals were recorded with a strip battery-operated chart recorder (Servogor, Leeds, UK) operated via batteries. The O_2 microsensor had a tip diameter of 6 μm, a stirring sensitivity of ∼2% and a response time, t_{90}, of 0.2 s. The O_2 microsensor was linearly calibrated on site from readings of microsensor current in the overlying water and in the anoxic part of the mat (2% O_2). Dissolved O_2 concentrations in the overlying water were determined by Winkler titration [16]. Experimental light–dark shifts for in situ measurements of oxygenic gross photosynthesis [17] were performed with a custom-made, light-impermeable box, which was deployed by avoiding physical contact with the sensor and thus disturbance of microsensor readings.

2.4. Spectral scalar irradiance measurements with fiber-optic microprobes

Mat samples were collected in February 2001 for spectral scalar irradiance measurements under controlled conditions in a laboratory. Due to the time difference

between the sampling times (May 2000 for all other analyses), some seasonal changes in the small-scale vertical location of the different photosynthetic microorganisms in the mat cannot be excluded, despite a similar macroscopic appearance of the mat at both times. For spectral light measurements, a fiber-optic scalar irradiance microprobe [18], was connected to a sensitive fiber-optic diode array spectrometer with a spectral range of 250–950 nm (PMA-11, Hamamatsu Photonics, Toyooku, Japan). Profiles of spectral scalar irradiance were measured in the mat by stepwise inserting the microprobe with a motor-driven micromanipulator (Märzhäuser, Eugene, USA) at a zenith angle of 140° relative to the incident light beam. The downwelling spectral scalar irradiance at the mat surface was measured by positioning the scalar irradiance microprobe over a black light trap at the same position relative to the incident light as the mat surface. Scalar irradiance spectra in the mat were normalized to the downwelling spectral scalar irradiance at the mat surface. Attenuation spectra of scalar irradiance were calculated over discrete depth intervals from the scalar irradiance profiles according to Kühl and Fenchel [19].

2.5. Analysis of fatty acids, hydrocarbons, alcohols and alkenones

The microbial mat samples were extracted after homogenization with methanol, dichloromethane and *n*-hexane. Fatty acids were separated from the extracts after saponification. Afterwards the neutral lipids were fractionated by column chromatography with silica and alumina into different compound classes. Hydrocarbons and polar fractions were analyzed by gas chromatography (GC) and gas chromatography mass spectrometry (GC-MS) after derivatisation. The methodology was described in detail recently by Wieland et al. [4].

2.6. Confocal laser scanning microscopy

The mat samples were analyzed with a microscope (Olympus BH2, Tokyo, Japan) and a confocal laser-scanning microscope (Leica TCS 4d, Heidelberg, Germany) equipped with an argon–krypton laser. For confocal analysis, slices of defined dimensions were placed on cavity slides, sealed with cover slips and observed under an excitation beam of 568 nm. Pigment fluorescence emission was detected with a 590 nm long pass filter. Different 512×512 pixel confocal images in two (optical sections) and three-dimensions (sum of projections and stereoscopic images) were obtained from these samples. The cyanobacteria were identified using different morphological criteria according to Castenholz [20], i.e. diameter (μm), cell division patterns, and the presence or absence of a sheath for unicellular morphotypes. Presence of septation and gas vacuoles was also considered for filamentous cyanobacteria. In addition, the abundance of each cyanobacterial genera was determined by counting the different morphotypes obtained from CLSM images. A total of 663 filamentous and 237 unicellular cyanobacteria were analyzed.

2.7. DGGE analysis

Genomic DNA was extracted from the mat samples using the UltraClean Soil DNA Isolation Kit (Mobio Laboratories, Carlsbad, USA) according to manufacturer's instructions. Serial dilutions of genomic DNA (up to 10^{-4}) were made in sterile water and stored at −20 °C. To specifically amplify the 16S rRNA gene fragments of oxygenic phototrophs, 1 or 2 μl of the DNA dilutions were used as templates in 50 or 100 μl PCR reactions using primer pair CYA359F + GC/CYA781R and PCR conditions as described by Nübel et al. [21]. The two different reverse primers CYA781RA and CYA781RC were added in separate PCR reactions. DGGE was performed according to Schäfer and Muyzer [22] with conditions optimized for the oxygenic phototroph specific PCR fragments [21], on 1 mm thick 6% acrylamide/bisacrylamide gels with urea-formamide (UF) gradient of 20–80%. On top of the gradient gel, an acrylamide gel without UF was cast to obtain loading slots. Gels were run in TAE (40 mM Tris-acetate pH 8.5, 1 mM EDTA) buffer for 3.5 h at 200 V and at a constant temperature of 60 °C. Subsequently, the gels were stained in an ethidium bromide solution (0.5 $\mu g\,ml^{-1}$) and inspected under UV illumination using a Fluor-S Multi Imager (Bio-Rad, Hercules, USA). Contrast and brightness of the photographs were optimized using Adobe PhotoShop software (Adobe, San Jose, USA). DNA fragments separated by DGGE were excised from the gel [23], re-amplified, purified using the Qiaquick gel extraction kit (Qiagen, Hilden, Germany), and then sequenced. Purified bands were sequenced in two directions using the BigDye Terminator cycle sequencing kit (Applied Biosystem, Foster City, USA) on an ABI PRISM 310 genetic analyzer (Applied Biosystem). Close relatives to consensus sequences were searched in the GenBank Database maintained by the NCBI using BLAST search [24]. Subsequently, new sequences and their closest relatives were added to the ARB database [25] and aligned using the automatic alignment tool. Alignments were then checked and corrected manually taking the alignments of oxygenic phototrophs that were already in the ARB database as templates. Phylogenetic analysis was performed in ARB using several different algorithms (e.g., maximum parsimony, neighbour-joining, maximum likelihood) to check the consistency of the tree structure. All three methods gave similar topology. Neighbour joining was used to draw the phylogenetic tree. The GenBank accession numbers of each

partial 16S rRNA gene clone (SdG1 to SdG7) are AY393850 to AY393856.

2.8. T-RFLP analysis

The upper 2 mm of the mat cores were sliced into 200 μm sections with a cryomicrotome (MICROM GmbH, Walldorf, Germany), and from the third mm into 500 μm section for vertical depth resolution. The mat slices were ground together with liquid nitrogen in a mortar with a pestle and genomic DNA was extracted using the UltraClean Soil DNA isolation kit (MoBio Laboratories, Carlsbad, USA) according to the manufacturer. All extracted genomic DNA samples were stored at −20 °C until further processing. T-RFLP analysis was performed with different primer sets, 8f–926r [26,27], 8f–SRB385 [28], and pb557f–pb750r [29], according to the experimental conditions described in Wieland et al. [4]. Respectively, these primer sets targeted the whole bacterial community, the sulfate-reducing bacteria (SRB), and the phototrophic anoxygenic bacteria (PAB). Restriction enzymes used in T-RFLP analysis were *Hae*III and *Rsa*I (New England Biolabs, Beverly, UK), for analysis of the entire bacterial diversity, and *Hae*III and *Hin6*I for the SRB and PAB. Triplicates for each layer were analyzed to avoid analytical artifacts and assure the reproducibility of the method. Dominant terminal restriction fragments (T-RFs) over 100 fluorescent units in intensity and present in each replicate sample were selected. The size of each T-RF was determined according to molecular weight standard TAMRA 500 (Applied Biosystem) with an acceptable error of ±1 bp. From T-RF values, genus or species identification were made by predicted digestions using the TAP-TRFLP program of the RDP (Ribosomal Database Project) web site (http://rdp.cme.msu.edu/) [30]. T-RFLP profiles were normalized by calculating relative abundances of each T-RFs from height fluorescence intensity. Combining data from each restriction enzyme, we compared normalized T-RFLP profiles by correspondence factorial analysis (CFA).

2.9. Correspondence factorial analysis

CFA is an ordination method by similarity matrix that reduces in two or three dimensions the dispersion diagram of samples compared (in this case T-RFLP profiles). Axes correspond to synthetic variables (T-RFs) and their influence (percent relative abundance) in the distribution of samples analyzed [31]. Using CFA, two-dimensional plots were prepared, showing variance within data sets on a series of axes. To clearly present the results two graphs were constructed using MVSP v3.12d software (Kovach Computing Service, Anglesey, Wales) [32]. One graph was constructed for T-RFs (or OTUs, operational taxonomic units) and the other for layers using the same axis.

The fact that some samples do not appear in the CFA graph is due to insufficient DNA yield for some analyses.

3. Results

3.1. Description and environmental conditions of the microbial mat

3.1.1. Structure of the microbial mat

The microbial mat was composed of three distinct colored layers. An upper, approximately 2 mm thick, brown–green colored layer was composed of filamentous cyanobacteria morphologically related to the genus *Microcoleus*, and of unicellular cyanobacteria similar to the form genus *Synechocystis*. Under this dense cyanobacterial layer, an ~1 mm thick purple layer was composed of purple non-sulfur bacteria morphologically resembling members of Rhodospirillaceae and Chromatiaceae families (R. Guyoneaud, personal communication). Beneath these two layers a black zone of more than 1 cm occurred with iron sulfide precipitates, indicating intense sulfate-reduction activity. The physical and chemical parameters measured in the sampling site (Table 1) were generally constant.

Table 1
Comparison of physical and chemical parameters in the water column of the sampling site measured at 15 h each day of sampling

Dates	Temperature (°C)	O_2 (μmol l^{-1})	Redox (mV)	pH	Salinity (‰)
23.05.00	20	17.0 ± 0.1	+3[a] ± 1 −4[b] ± 1	8.39 ± 0.02	103 ± 1
25.05.00	23	ND	+90[a] ± 1 ND[b]	8.50 ± 0.02	75 ± 1

ND, not determined.
[a] Surface.
[b] 10 mm depth.

3.1.2. Depth profiles of O_2, gross photosynthesis, and spectral scalar irradiance

High O_2 consumption in the mat led to a low O_2 concentration and O_2 penetration in situ during the night (5:32 h, 17 °C, 94‰ (v/w)), confining the oxic zone to the top 0.2 mm of the mat (Fig. 1). In the afternoon (15:50 h, 30 °C, 100‰ (v/w)), high rates of oxygenic photosynthesis led to a strong increase in O_2 concentration both in the overlying water and within the mat. The O_2 penetration depth in the mat increased to 2 mm. Gross oxygenic photosynthesis was measurable in the top 0.6 mm of the mat with a peak in photosynthetic activity at 0.3–0.6 mm depth. An important photosynthetic activity at 0.3–0.6 mm depth indicated the presence and/or activities of oxygenic phototrophs in the upper mat layers.

From measured spectral scalar irradiance profiles, distinct spectral regions of pronounced absorption could be ascribed to the presence of different pigments (Fig. 2, upper graph). The presence of cyanobacteria led to pronounced scalar irradiance minima at around 630 and 680 nm, corresponding to phycocyanin and chlorophyll *a* (Chl *a*) absorption, respectively. The scalar irradiance minima in the region between 800 and 900 nm corresponds to bacteriochlorophyll *a* (Bchl *a*) absorption, indicating the presence of purple bacteria. A shoulder at 740–750 nm indicated some absorption by Bchl *c* present in green photosynthetic bacteria. In the spectral region of 400–550 nm, scalar irradiance was strongly attenuated due to Chl *a* and carotenoid absorption.

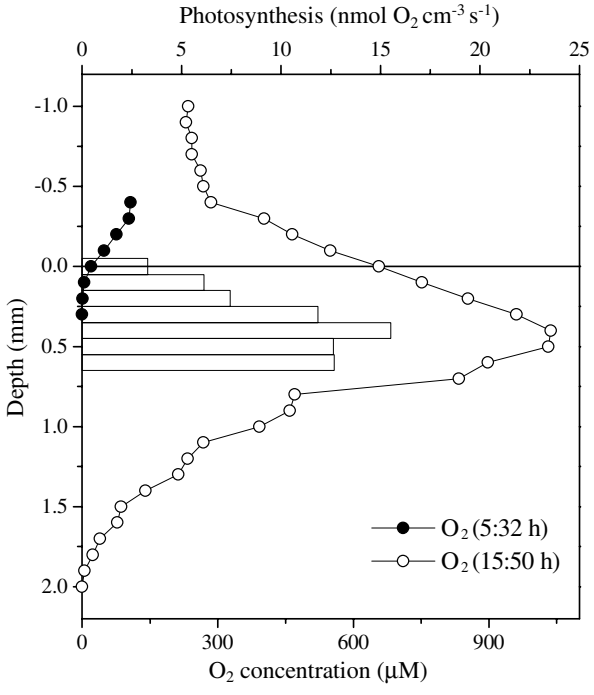

Fig. 1. In situ depth profiles of O_2 and gross photosynthesis (bars) measured during the afternoon (15:50 h) and night (5:32 h) in mats from a pre-concentration pond of the Salins-de-Giraud saltern.

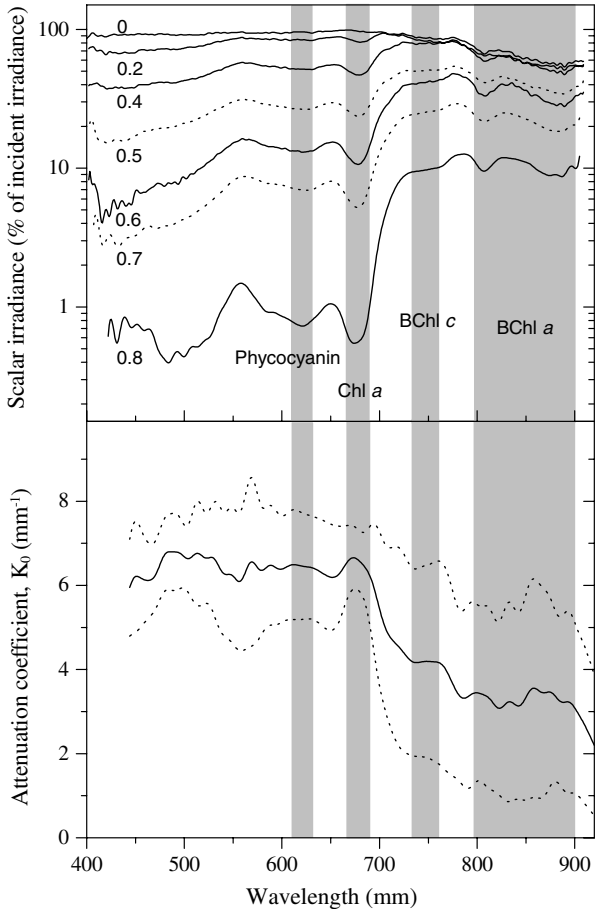

Fig. 2. Depth profiles of spectral scalar irradiance in the Camargue mat normalized to the downwelling spectral scalar irradiance at the mat surface (upper graph). Numbers indicate depth (mm). Average attenuation spectrum of scalar irradiance over the depth interval of 0–0.8 mm (lower graph), calculated from the profile shown in the upper graph. Broken lines indicate the standard deviations of the attenuation coefficients, K_0.

Absorption by Chl *a*, phycocyanin, Bchl *a*, and Bchl *c* occurred in all mat layers within the top 0.8 mm of the mat, indicating a homogeneous distribution of these photosynthetic groups. However, the spectral scalar irradiance in the wavelength regions of Chl *a*, phycocyanin and carotenoid absorption were more strongly attenuated than wavelengths corresponding to Bchl *a* and Bchl *c* absorption (Fig. 2, lower graph), indicating as expected a dominance of cyanobacteria in the surface layer of the mat.

3.2. Bacterial community composition in the top active layers of the microbial mat

3.2.1. Bacterial community composition estimated by biomarkers

Fatty acids were the major lipid compounds found in the microbial mat. Their distribution essentially encompassed C_{14}–C_{22} homologues, namely *n*-hexadec-9(Z)-enoic, *n*-hexadecanoic, *n*-octadec-9(Z)-enoic,

n-octadec-11(Z)-enoic, *iso*-pentadecanoic and *anteiso*-pentadecanoic acids (Fig. 3(a)), typically representative of algal and bacterial communities [33,34].

Cyclopropylnonadecanoic acid was also a major compound in the distribution of fatty acids. This compound is abundant in purple phototrophic bacteria such

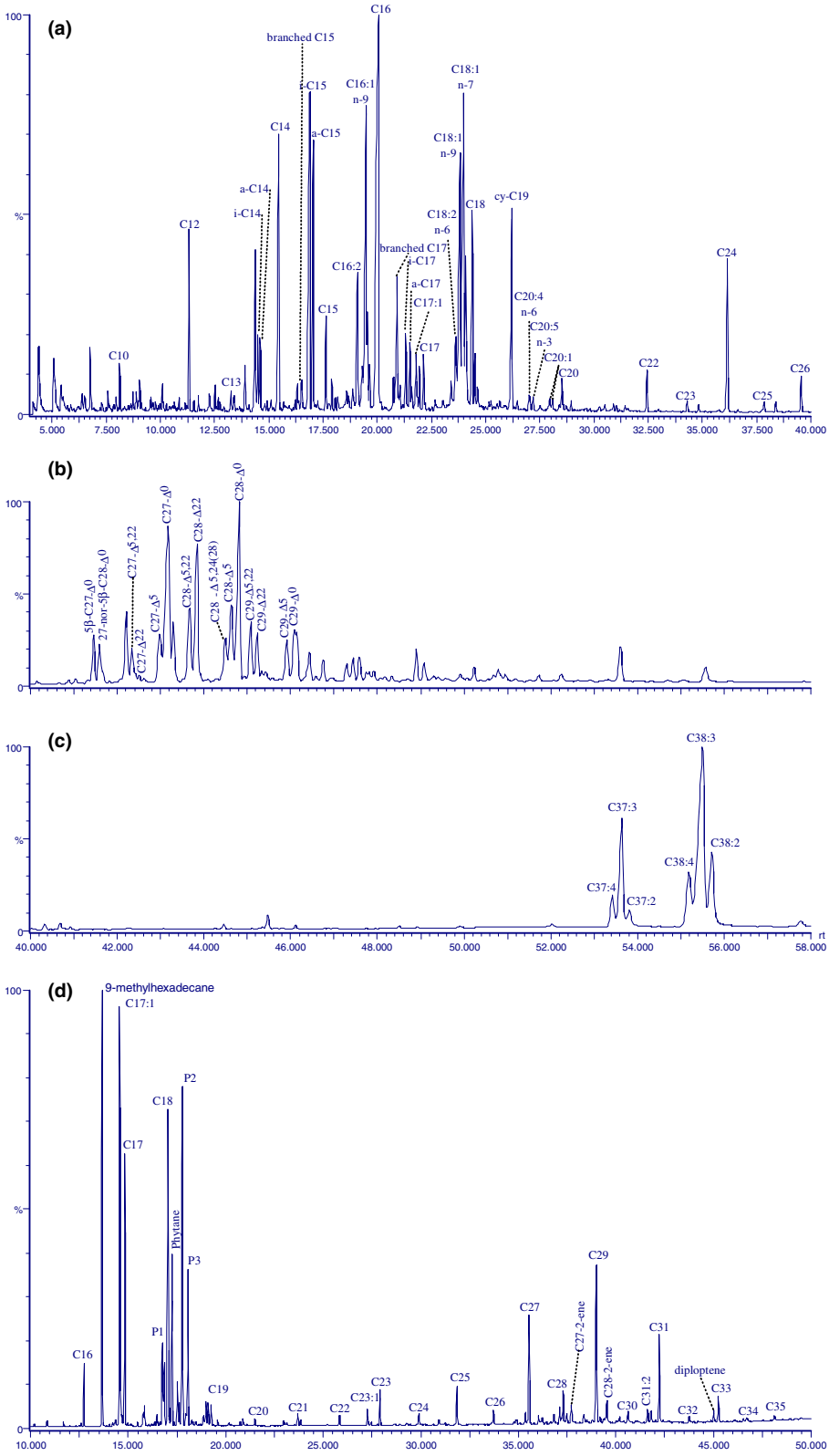

Fig. 3. Gas chromatographic profiles showing the major (a) fatty acids, (b) alcohol and (c) alkenone fractions, (d) hydrocarbons (P1, P2, P3 phytenes) from Salins-de-Giraud microbial mat.

as *Rhodobacter* and *Ectothiorhodospira* where it occurs together with significant amounts of *n*-octadec-11(Z)-enoic acid [35]. *Iso*- and *anteiso*-pentadecanoic acids are abundant in SRB and sulfur-oxidizing bacteria such as *Thiomicrospira* [35]. The high abundance of *iso*- and *anteiso*-pentadecanoic acids, as well as of cyclopropyl-nonadecanoic and *n*-octadec-11(Z)-enoic acids likely reflects the dominance of two different populations exchanging hydrogen sulfide, which could be sulfate-reducing and purple phototrophic bacteria, respectively.

n-Heptadecane and *n*-heptadecenes were the main hydrocarbons (Fig. 3(c)). These compounds are generally found in cyanobacteria [36,37] or in phototrophic eukaryota [38]. Other hydrocarbons specific of cyanobacterial inputs, such as 9-methylhexadecane, were also found in major proportions, indicating the dominance of cyanobacteria in this mat.

The sterol distribution of this mat showed minor proportions of sterols having the unsaturated positions at Δ^5, Δ^{22} and $\Delta^{5,22}$ (Fig. 3(b)), which could originate from cyanobacteria [37,39,40], Chlorophyta [41,42], or diatoms [42–44]. However, the common diatom marker 24-methylcholesta-5,24(28)-dien-3β-ol [42–44] was only found in minor proportion.

Phyt-1-ene, which occurred together with other phytene homologues, also constituted one of the major hydrocarbon groups (Fig. 3(d)). These hydrocarbons are characteristic for methanogenic bacteria [45].

3.2.2. Diversity of oxygenic phototrophs

Confocal laser scanning microscopy and molecular techniques were used to identify the cyanobacteria of the Camargue microbial mat. Using CLSM, both filamentous and unicellular cyanobacteria were found in the mat (Table 2 and Fig. 4). Filamentous types were the most abundant, accounting for 73.6% of the total cyanobacteria present (Table 2). *Microcoleus chthonoplastes* (Fig. 4(b)) dominated the filamentous cyanobacterial community, as typically found in hypersaline mats [1,46,47]. *Halomicronema excentricum*, characterized by thin filaments and cylindrical shape (less than 1 μm wide trichomes) (Fig. 4(c)) [48], and another filamentous cyanobacterium (Fig. 4(c)) with thin filaments and short trichomes that could not be identified, were the second most frequent filamentous cyanobacteria. *Leptolyngbya* sp., *Limnothrix* sp. and *Pseudanabaena* sp. filaments detected in this study at abundances of 9.9% and 6.6%, respectively, have also been found in other mats as well, e.g. from the Ebro delta [1,46,47] and the Orkney Islands [4]. Unicellular cyanobacteria *Chroococcus* sp., *Microcystis* sp. and members of *Synechocystis* (Fig. 4(d)) and *Gloeocaspsa* groups represented 26.4% of the total cyanobacteria in the Camargue mat (Table 2).

In addition to CLSM analysis, a molecular approach was used to describe the oxygenic phototroph community composition. PCR amplified 16S rRNA gene products specific for cyanobacteria, were separated by DGGE. Fifteen different bands were counted, and the major bands were excised from the gel (bands 1–7 in Fig. 5(a)) and retrieved for DNA sequencing. In combination with CLSM, phylogenetic analysis of these sequences (SdG1 to SdG7 in Fig. 5(b)) showed that the pristine hypersaline Camargue mat was dominated by the filamentous cyanobacteria: genera *Microcoleus* (SdG5 and SdG6), *Oscillatoria* (SdG3) and *Leptolyngbya* (SdG7 in Fig. 5(b)). Other cyanobacteria composing this mat were related to the unicellular *Pleurocapsa* sp. (SdG1), *Calotrix* sp. (SdG4), and *Phormidium* sp. (SdG2).

3.2.3. Bacterial community structure at a microscale level

The organization and composition of the bacterial community in the mat was investigated by T-RFLP

Table 2
Morphological identification of cyanobacteria in microbial mats of Salins-de-Giraud by CLSM according to Castenholz [20], and their relative abundances

Microorganisms	Diameter (μm)	Septation	Gas vacuole	Sheath	Cell division	Abundance (%)
Filamentous cyanobacteria						
Microcoleus chthonoplastes	3.13–3.75	+	–	+	Perpendicular division	20.8
Halomicronema excentricum	0.96	+	–	+	Perpendicular division	13.2
Unidentified	<1.25 (short filaments)	+	–	+	Perpendicular division	13.2
Leptolyngbya sp.	<1 (large filaments)	+	–	+	Perpendicular division	9.9
Limnothrix sp.	1.25	+	–	+	Perpendicular division	9.9
Pseudanabaena sp.	2.5	+	+	+	Perpendicular division	6.6
Unicellular cyanobacteria						
Synechocystis-group (marine cluster)	3.5 × 3.5	–	–	+ (thin)	2 or 3 planes	6.6
Gloeocapsa-group	4 × 14	–	–	+	2 or 3 planes	6.6
Chroococcus sp.	19 × 28	–	–	+	2 planes	6.6
Microcystis sp.	1.9 × 1.9	–	–	+	Binary fission in different planes	6.6

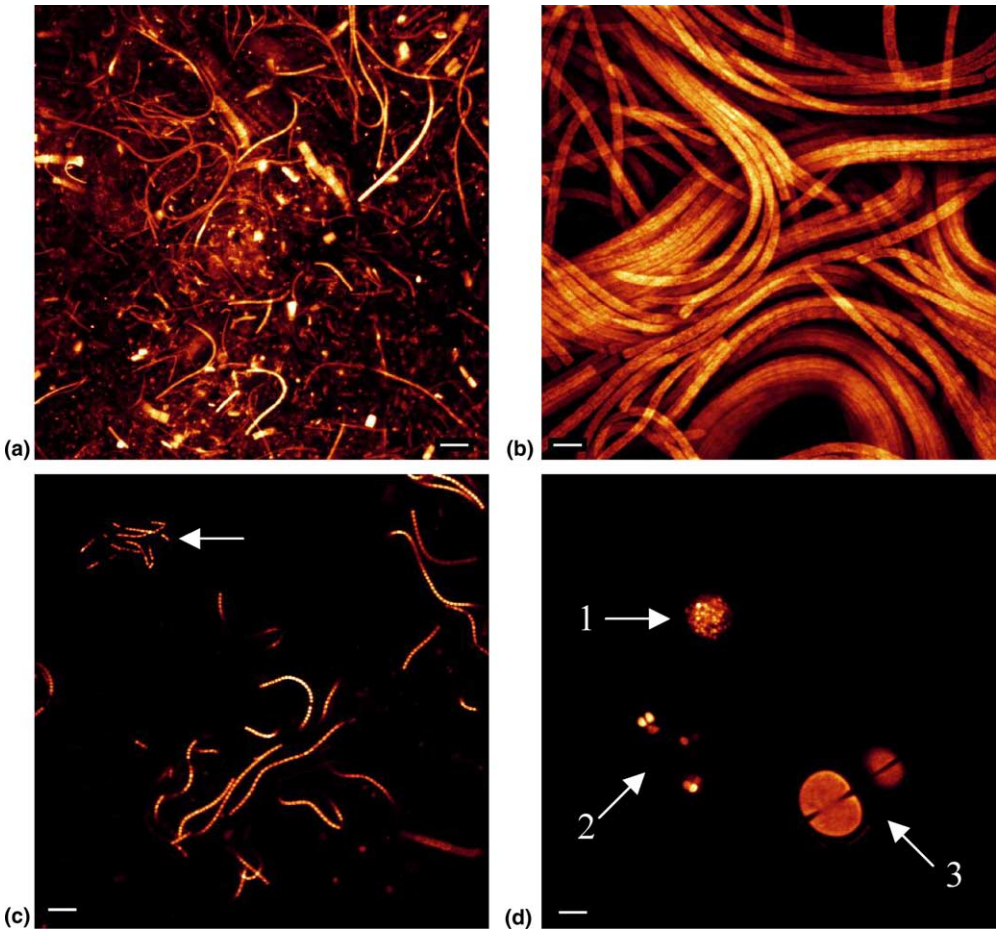

Fig. 4. CLSM images in Salins-de-Giraud microbial mat. (a) *Leptolyngbya* sp., (b) *Microcoleus chthonoplastes,* (c) *Halomicronema excentricum* and the unidentified filaments (indicated by arrow), (d) 1. *Microcystis* sp., 2. *Synechocystis*-group., 3. *Chroococcus* sp. (c) and (d) images are photographic compositions. Scale bar = 10 μm.

using the eubacterial primer set 8f-926r [26,27], targeting a partial sequence of the 16S rRNA gene. For each microlayer within the top 3 mm of the mat, and of the underlying layer, characteristic T-RFLP profiles (approximately 35 T-RFs with *Hae*III digestion) were obtained (data not shown). A CFA combining the data from *Hae*III and *Rsa*I T-RFLP profiles revealed a particular distribution in three zones: a surface layer (0–0.2 mm), a large mid layer (0.2–3 mm), and a deeper region (underlying layer) (Fig. 6(a)). This distribution was mostly explained by the first axis (27.8%) particularly for the deep third millimeter. Plots of T-RFs in Fig. 6(b) showed that T-RF 58 bp (*Rsa*I), presumably *Desulfomicrobium baculatum,* and T-RFs 205 and 244 pb (*Hae*III), presumably members of the genera *Desulfobulbus* and *Streptomyces* respectively, were dominant in this deeper zone. In contrast, the structure of the surface mat (0–0.2 mm) was explained by the second axis (11.8%, Fig. 6(a)), which was influenced by T-RFs of 125 bp (*Rsa*I digest), 200 and 297 bp (*Hae*III digest) (Fig. 6(b)). These T-RFs that match members of the *Neisseria, Chloroflexus* and*Mycoplasma* genera were particularly present in this surface layer.

SRB were accessed by T-RFLP using the specific primer pair 8f–385r [28], and two restriction enzymes *Hae*III and *Hin*6I. The CFA of this data set also showed a specific distribution of the SRB. Particularly, two distinct SRB communities were characteristic of the deeper layer (2.5–3 mm) and of the layer at 1.4–1.6 mm (Fig. 7(a)). This later layer seemed to be independent, since the first axis (40.7%) alone explained the distinct structure of the mid layer. Fig. 7(b) shows that this mid layer was characterized by many T-RFs. Among them, T-RFs of 200 and 270 bp (*Hae*III) that could be related to genera *Desulfovibrio* and *Desulfobacter*, respectively, were dominant. The composition of the third millimeter of the mat was essentially explained by the second axis (14.8%, Fig. 7(a)), which was influenced by many T-RFs (Fig. 7(b)). Among them, T-RFs of 72 and 197 bp (*Hae*III) and of 55 bp (*Hin*6I) were dominant. The

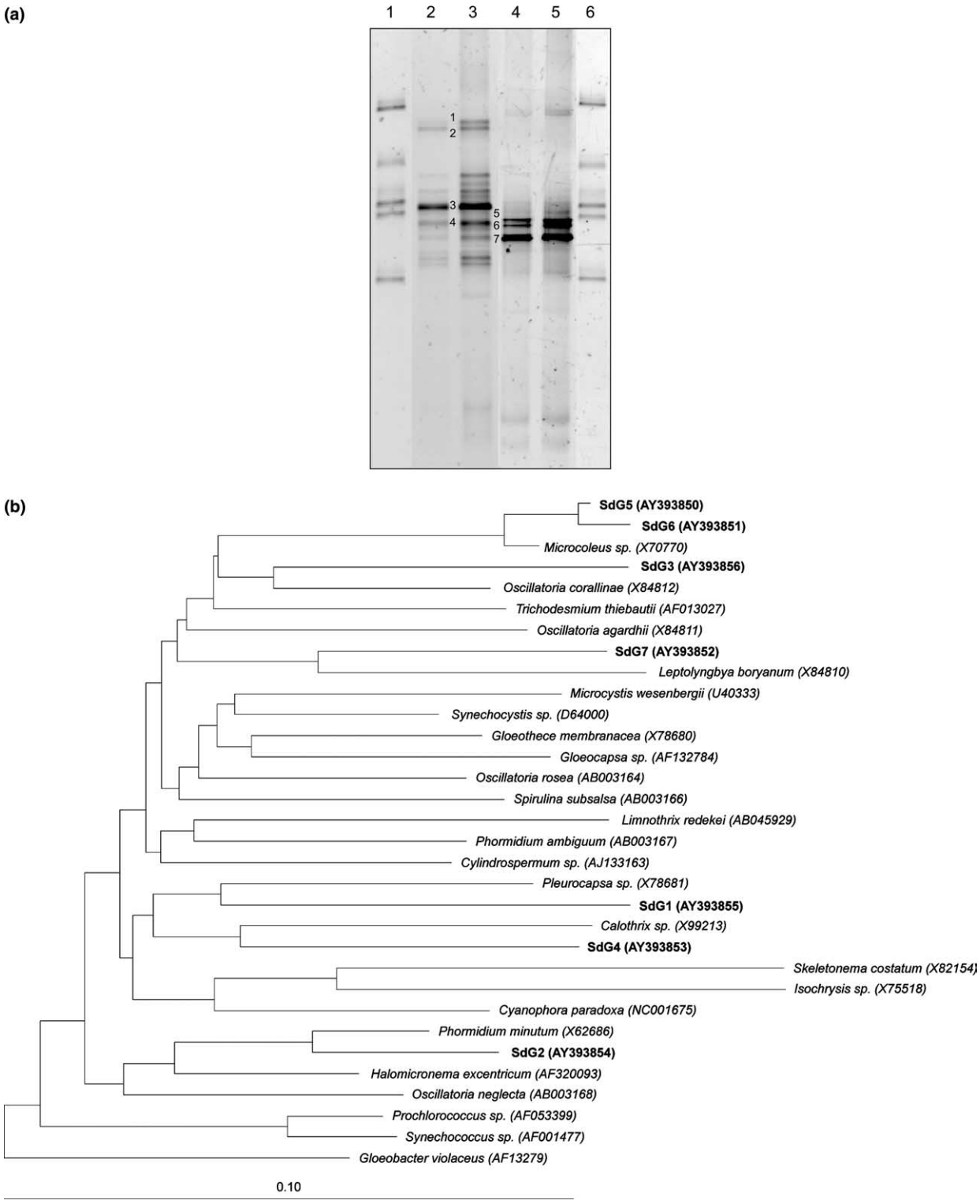

Fig. 5. (a) DGGE analysis of 16S rRNA gene fragments of oxygenic phototrophs. The PCR products were obtained with two different primer sets and genomic DNA from the microbial mat of Salins-de-Giraud (SdG). Lanes 1 and 6, marker fragments; lanes 2 and 3, PCR products obtained with primers CYA359F and GC/CYA781Rb; lanes 4 and 5 PCR products obtained with primers CYA359F + GC/CYA781Ra. 300 ng PCR product was loaded in each lane. The numbers in figures refer to bands that were excised from the gel, sequenced and used for phylogenetic analysis. (b) Neighbour-joining phylogenetic tree based on 16S rRNA gene sequence data showing the affiliation of predominant oxygenic phototrophs (i.e., cyanobacteria and diatoms) in the microbial mat of Salins-de-Giraud. Sequences determined in this study are shown in bold. The consistency of the tree structure was checked using several different algorithms. The sequences of *Thermus aquaticus* and *Chloroflexus aurantiacus* were used as the outgroup, but were pruned from the tree. The scale bar represents 10% estimated sequence divergence.

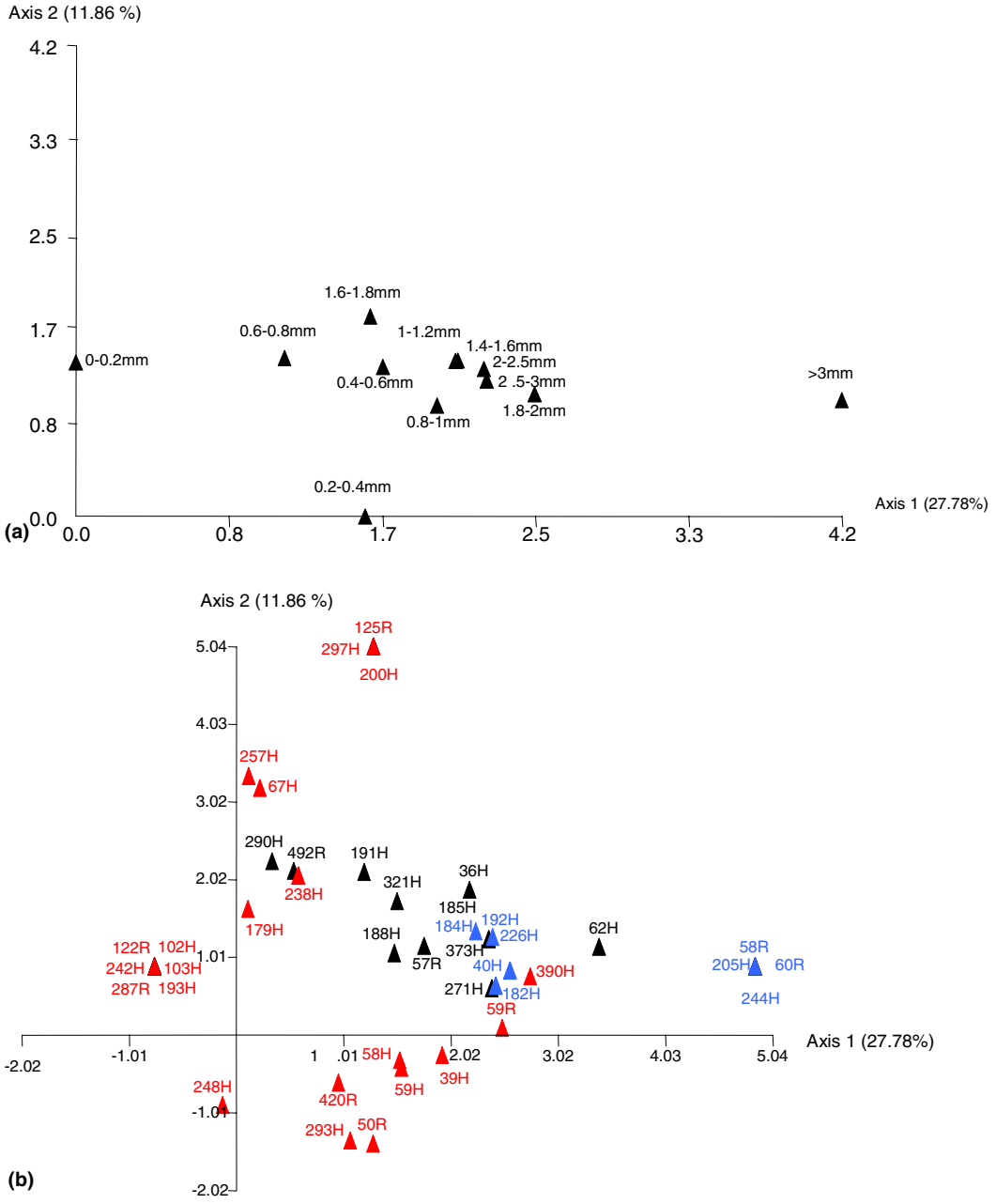

Fig. 6. CFA of the whole bacterial communities. (a) CFA of each layer of the 3 mm of Salins-de-Giraud microbial mat. Each black triangle was represented by a 5′ end T-RFLP pattern corresponding to the combined digests *Hae*III and *Rsa*I of the 16s rRNA genes. (b) CFA of variables, i.e., T-RFs derived from the CFA in panel (a). Each number corresponds to the T-RF length in base pairs. Letters H and R, after this number, correspond to *Hae*III and *Rsa*I T-RFs, respectively. Red and blue triangles correspond to T-RFs specific from the oxic (<2 mm) and anoxic zone (>2 mm) of the mat, respectively. Black triangles correspond to T-RFs non-specific from the mat zonation.

T-RF of 72 bp may possibly represent some *Desulfovibrio* communities.

In addition to SRB communities, the PAB were also investigated in the same layers. Their presence in the mat was detected with the primer pair pb557f–pb750r [29], targeting the *pufM* gene, which encodes a subunit of the photosynthetic center of purple sulfur and non-sulfur bacteria. CFA on T-RFLP patterns of these PAB communities revealed their organization in five layers through the top 3 mm of the mat (Fig. 8(a)). The distribution of the layers from 0.2 to 0.4 mm and from 0.4 to 1.8 mm was explained by the first axis (38.4%) corresponding to T-RF (199 pb, *Hae*III) possibly related to *Halochromatium salexigens* (Fig. 8(b)). The three other layers, from 0 to 0.2 mm, from 1.8 to 2 mm, and from 2.5 to 3 mm, were mostly influenced by the second axis

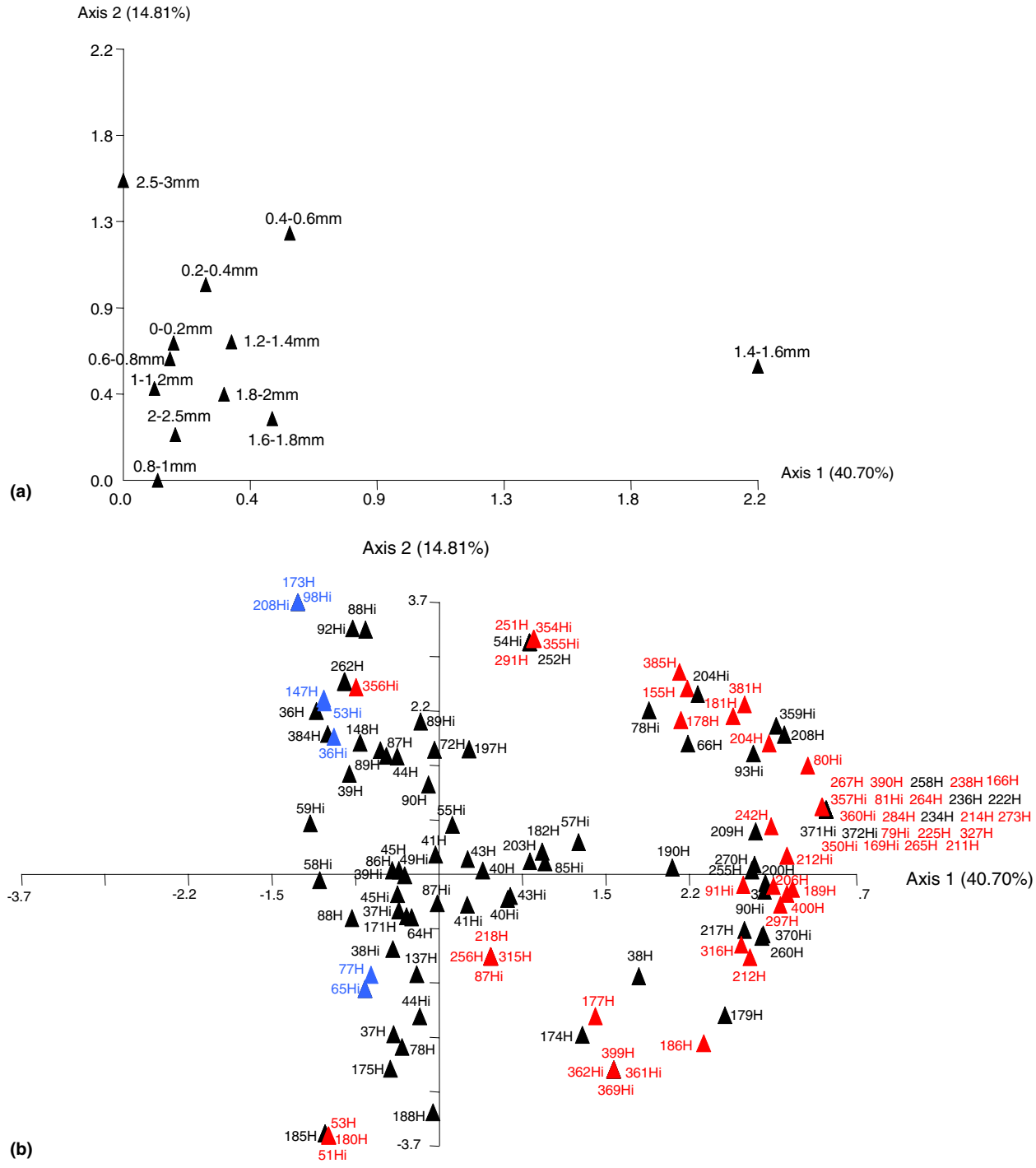

Fig. 7. CFA of the sulfate-reducing communities. (a) CFA of each layer of the 3 mm of Salins-de-Giraud microbial mat. Each black triangle was represented by a 5′ end T-RFLP pattern corresponding to the combined digests *Hae*III and *Hin*6I of the 16s rRNA genes. (b) CFA of variables, i.e., T-RFs derived from the CFA in panel (a). Each number corresponds to the T-RF length in base pairs. Letters H and Hi, after this number, correspond to *Hae*III and *Hin*6I T-RFs, respectively. Red and blue triangles correspond to T-RFs specific from the oxic (<2 mm) and anoxic zone (>2 mm) of the mat, respectively. Black triangles correspond to T-RFs non-specific from the mat zonation.

(12%). The CFA plots (Fig. 8(b)) showed that this second axis was explained mainly by the presence of the major T-RF of 137 bp (*Hin*6I) potentially corresponding to *Roseospira marina*.

4. Discussion

The investigated photosynthetic microbial mat showed a spatial distribution of different functional

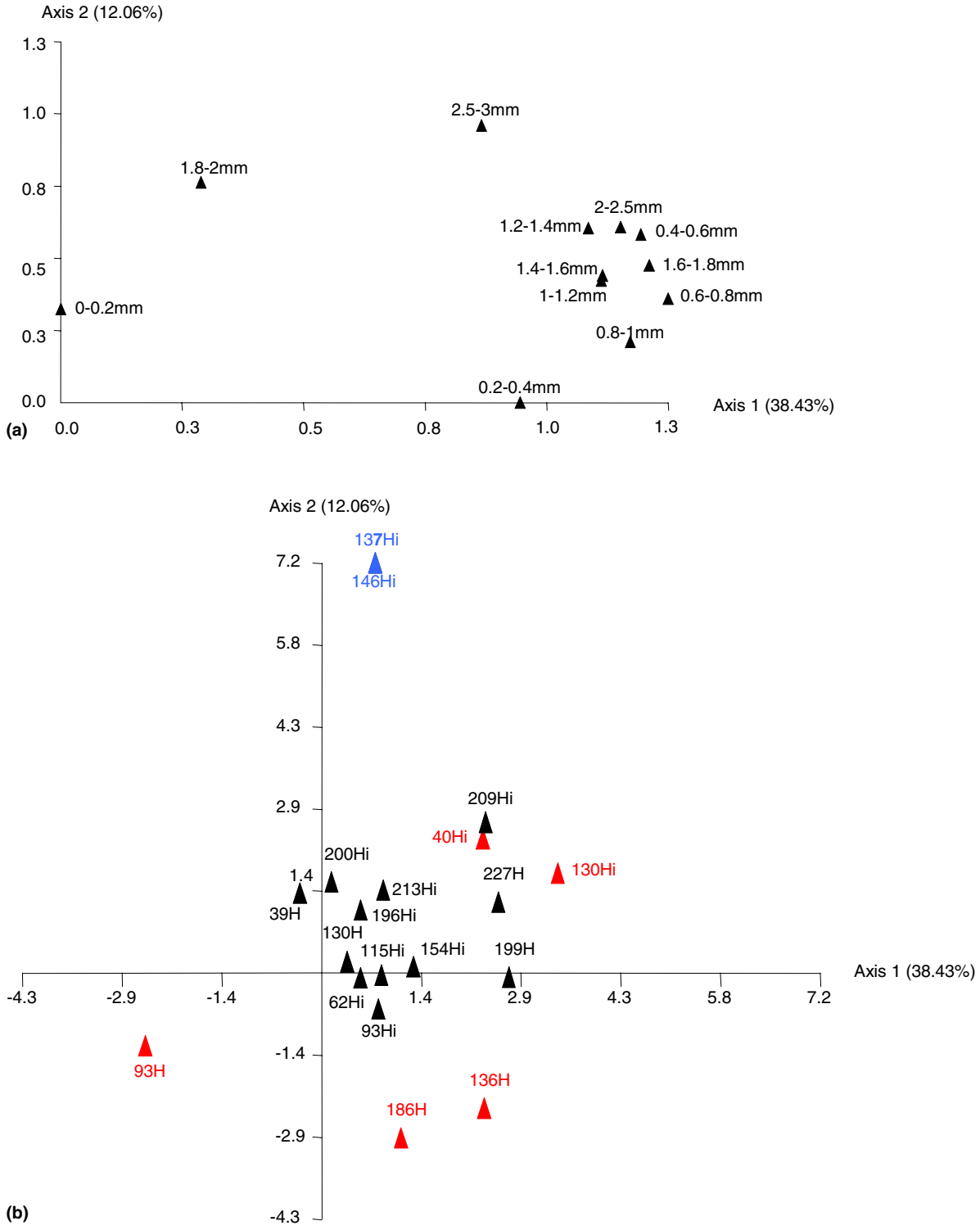

Fig. 8. CFA of the phototrophic anoxygenic communities. (a) CFA of each layer of the 3 mm of Salins de Giraud microbial mat. Each black triangle was represented by a 5′ end T-RFLP pattern corresponding to the combined digests *Hae*III and *Hin*6I of the PufM encoding gene. (b) CFA of variables, i.e., T-RFs derived from the CFA in panel (a). Each number corresponds to the T-RF length in base pairs. Letters H and Hi, after this number, correspond to *Hae*III and *Hin*6I T-RFs, respectively. Red and blue triangles correspond to T-RFs specific from the oxic (<2 mm) and anoxic zone (>2 mm) of the mat, respectively. Black triangles correspond to T-RFs non-specific from the mat zonation.

groups at the microscale level. As revealed by spectral scalar irradiance (Fig. 2), by CLSM (Table 2), and by DGGE (Fig. 5), the cyanobacteria were dominant and rather diverse photosynthetic microorganisms active in the first millimeter of the mat. Analyses of biomarkers (Fig. 3) corroborated these observations of a dominance

of oxygenic phototrophs, since major fatty acids (*n*-octadec-9(Z)-enoic acid), alcohols (5α(H)-stanols), and hydrocarbons (*n*-heptadecane, *n*-heptadecenes, and 9-methylhexadecane) found in this mat corresponded to cyanobacteria [49].

Identification of oxygenic phototrophs down to the genus or even species level was done by confocal laser scanning microscopy and sequencing analysis (PCR-DGGE-sequencing). Two dominant filamentous cyanobacteria *Microcoleus* sp. and *Leptolyngbya* sp. were identified by both techniques. Other oxygenic phototrophs were either identified by CLSM (*Halomicronema*, *Limnothrix*, *Pseudanabaena*, *Synechocystis* – group, *Gloeocapsa* – group, *Chroococcus*, and *Microcystis*) or by sequencing analysis (*Phormidium*, *Calotrix*, *Pleurocapsa*, *Oscillatoria*). Thus, the combination of both CLSM and DGGE was useful to fully describe the oxygenic phototrophic communities.

As described previously, bacterial biodiversity depends on gradient salinity, with a decreasing bacterial diversity when salinity increases [50–52]. However, in this investigated halophilic microbial mat, the diversity of oxygenic phototrophs is moderate in comparison to those previously described [53] with the dominance of *M. chthonoplastes* a typical inhabitant of halophilic microbial mat [54–56]. At higher salinities, other cyanobacterial morphotypes, like *Phormidium,* could be dominant [5].

Within the mat, analysis of biomarkers revealed the presence of purple bacteria like *Rhodobacter* and *Ectothiorhodospira*, and also of SRB. *Iso*- and *anteiso*-pentadecanoic acids are abundant in SRB and sulfur-oxidizing bacteria such as *Thiomicrospira* [35]. Cyclopropylnonadecanoic acid was also a major compound in the distribution of fatty acids. This compound is abundant in purple phototrophic bacteria such as *Rhodobacter* and *Ectothiorhodospira* where it occurs together with significant amounts of *n*-octadec-11(Z)-enoic acid [35]. The ratio between these two acids (0.5) could be related to the growth status of the microbial mat, with a high relative proportion of the cyclopropyl acid being indicative of stationary growth [57]. The high abundance of *iso*- and *anteiso*-pentadecanoic acids, as well as of cyclopropylnonadecanoic and *n*-octadec-11(Z)-enoic acids likely reflects the dominance of two different populations exchanging hydrogen sulfide, which could be sulfate-reducing and purple phototrophic bacteria, respectively. By the use of specific primer sets, T-RFLP allowed us to distinguish photosynthetic anoxygenic bacteria (PAB) and SRB organized in five and three distinct bacterial groups among the first 3 mm of this mat, respectively (Figs. 7 and 8).

Measurements of the spectral scalar irradiance revealed the presence of purple bacteria in the surface layer of the mat, especially in the zone at 0.5–0.8 mm depth (Fig. 2). This confirms the observation with T-RFLP, showing the presence of distinct populations at 0.4–1.8 mm. In contrast, only few PAB were observed in the upper layer (0–0.4 mm) (Fig. 8(a)). Therefore, the PAB developing at greater depths in the mat could be adapted to lower light intensities, as compared to the PAB community of the surface layer, since light is strongly attenuated in the mat (Fig. 2). Moreover, oxygen could also play a role in the stratification of the PAB, discriminating populations of different tolerance to the presence of oxygen, especially in the surface layer of the mat with high oxygen concentrations (Fig. 1).

We could demonstrate the presence of *Desulfobacter*-like and *Desulfovibrio*-like SRB, in the mid layer of the mat, corresponding to the fluctuating oxic and anoxic zone during the diel cycle (Fig. 1). Many *Desulfovibrio* species were isolated from the oxic zone of microbial mats, and were found to be able to tolerate and consume oxygen [58,59]. An oxygen tolerant SRB community that could not be correlated by T-RFLP to any known SRB inhabited the 1.6 mm top layer that is completely oxic during the day. Previous molecular studies have described the presence of *Desulfonema*-like species in the oxic surface layer of several microbial mats [60,61]. They were found to be metabolically versatile with a high affinity to oxygen. In the deeper 3 mm layer, our study showed that one SRB population was specific to the anoxic layer, indicating probably a high sensitivity to oxygen. Thus, T-RFLP analysis illustrated a vertical stratification of the SRB within the top 3 mm layers of the mat, that could be explained by their behavioral responses to oxygen including aggregation, migration to anoxic zones, and aerotaxis [58].

The microscale zonation of these populations is partly controlled by the microgradients of oxygen, sulfide and light. In the investigated mat, no free sulfide was measurable with microsensors (Fig. 2), but iron sulfide precipitates, and measurements of sulfate reduction rates (SRR) (Rod Herbert, unpublished results) indicated high bacterial sulfate reduction activity and subsequent precipitation of the produced sulfide by iron. Investigation of the biogeochemistry of the mat in year 2001 confirmed that this Camargue mat is characterized by high sulfate reduction rates and a high iron and FeS content [62]. Additionally, in this mat *Chloroflexus*-like bacteria, detected by T-RFLP, were found as important members in the surface layer community (Fig. 6). Their presence was also indicated by the BChl *c* absorption detected in the top layer of the mat (Fig. 2). These microorganisms could play an important role in hypersaline and iron-rich microbial mats [63].

Biomarkers also evidenced organic matter contributions to these microbial mats from other origins. Thus, C_{37}–C_{38} di-, tri- and tetra-unsaturated alkenones (Fig. 3(b)) are specific of Hapthophyceae [64,65]. However, their occurrence cannot be attributed to species typically

found in pelagic environments and are probably related to unknown species. Moreover, a distribution of C_{23}–C_{35} *n*-alkanes predominated by the odd carbon numbered homologues, namely C_{29}, C_{31} and C_{33}, was found. This distribution is representative of inputs from higher plants [66] and is currently found in microbial sediments from coastal environments [67]. The allochthonous origin of these *n*-alkanes is clear based on their biosynthetic origin. The absence of higher plants nearby hypersaline systems suggest that their presence in microbial mat systems such as the one in Camargue may reflect the influence of wind transported remains from nearby higher plants, as already observed in other hypersaline areas [67]. Further evidence of the external origin of these C_{23}–C_{35} *n*-alkanes has been obtained in other coastal Mediterranean systems from comparison of the δ^{13} C isotopic composition of these *n*-alkanes and in situ generated microbial mat lipids. Whereas the former exhibit the typical values of higher plant compounds, e.g. $<-20‰$, the latter reflect the intense use of CO_2 as consequence of the high productivity and therefore the δ^{13} C isotopic values are much heavier, $>-20‰$ [68].

5. Conclusions

The results presented here demonstrated a clear stratification of the main photosynthetic and sulfur bacterial populations in distinct and specific vertical microlayers according to their physiological characteristics. The first active millimeter of this photosynthetic microbial mat was dominated by filamentous cyanobacteria such as *M. chtonoplastes*. Beneath this cyanobacterial layer, sulfur oxidizing bacteria like *Thiomicrospira* were present. Although diverse anoxygenic phototrophic bacteria such as *Rhodobacter* and *Ectothiorhodospira* inhabited this mat, *H. salexigens* and *R. marina* were dominant in surface and deep zones, respectively. Sulfate reducing bacteria responsible of high sulfate reduction rates were distributed within the depth profile. *Desulfonema* dominated the oxic surface, *Desulfobacter* and *Desulfovibrio* the mid oxic–anoxic layer while oxygen sensitive SRB were located in the deeper zone. Others organisms such as algae and diatoms contributed to the microbial mat structure and development.

In man-made artificial salterns, where such a type of mat develops, environmental conditions can change dramatically on a short term [62]. The structures of bacterial communities in microbial mats have mainly been described globally at the macroscale level. In contrast, this study of the hypersaline Camargue microbial mat represents the first exhaustive investigation, which clearly shows the structure and the distribution of the main bacterial communities at the microscale level according to the microgradients of oxygen and light.

Acknowledgements

We acknowledge the financial support by the EC (MATBIOPOL project, grant EVK3-CT-1999-00010). The authors are grateful to the company of Salins-dumidi at Salins-de-Giraud for facilitating access to the salterns, sampling and field experiments. A.F. is partly supported by a doctoral grant from the general council of Atlantic Pyrenees. M.K. was supported by the Danish Natural Science Research Council (contract no. 9700549). Anni Glud is gratefully acknowledged for microsensor construction and assistance during the field experiment.

References

[1] Esteve, I., Martínez, M., Mir, J. and Guerrero, R. (1992) Typology and structure of microbial mats communities in Spain: A preliminary study. Limnetica 8, 185–195.
[2] Mir, J., Martínez-Alonso, M., Esteve, I. and Guerrero, R. (1991) Vertical stratification and microbial assemblage of a microbial mat in the Ebro Delta (Spain). FEMS Microbiol. Ecol. 86, 59–68.
[3] van Gemerden, H., Tughan, C.S., de Wit, R. and Herbert, R.A. (1989) Laminated microbial ecosystems on sheltered beaches in Scapa Flow, Orkney Islands. FEMS Microbiol. Lett. 62, 87–101.
[4] Wieland, A., Kühl, M., McGowan, L., Fourçans, A., Duran, R., Caumette, P., Garcia De Oteyza, T., Grimalt, J.O., Solé, A., Diestra, E., Esteve, I. and Herbert, R.A. (2003) Microbial mats on the Orkney islands revisited: microenvironment and microbial community composition. Microbial Ecol. 46, 371–390.
[5] Caumette, P., Matheron, R., Raymond, N. and Relexans, J.C. (1994) Microbial mats in the hypersaline ponds of Mediterranean salterns (Salins-de-Giraud, France). FEMS Microbiol. Ecol. 13, 273–286.
[6] Giani, D., Seeler, J., Giani, L. and Krumbein, W.E. (1989) Microbial mats and physicochemistry in a saltern in the Bretagne (France) and in a laboratory scale saltern model. FEMS Microbiol. Ecol. 62, 151–162.
[7] van Gemerden, H. (1993) Microbial mats: A joint venture. Marine Geol. 113, 3–25.
[8] Revsbech, N.P., Jørgensen, B.B., Blackburn, T.H. and Cohen, Y. (1983) Microelectrode studies of the photosynthesis and O_2, H_2S and pH profiles of a microbial mat. Limnol. Oceanogr. 28, 1062–1074.
[9] Mouné, S., Caumette, P., Matheron, R. and Willison, J.C. (2003) Molecular sequence analysis of prokaryotic diversity in the anoxic sediments underlying cyanobacterial mats of two hypersaline ponds in Mediterranean salterns. FEMS Microbiol. Ecol. 44, 117–130.
[10] Mouné, S., Eatock, C., Matheron, R., Willison, J.C., Hirschler, A., Herbert, R. and Caumette, P. (2000) *Orenia salinaria* sp. nov., a fermentative bacterium isolated from anaerobic sediments of Mediterranean salterns. Int. J. Syst. Evol. Microbiol. 50 (Pt 2), 721–729.
[11] Mouné, S., Manac'h, N., Hirschler, A., Caumette, P., Willison, J.C. and Matheron, R. (1999) *Haloanaerobacter salinarius* sp. nov., a novel halophilic fermentative bacterium that reduces glycine-betaine to trimethylamine with hydrogen or serine as electron donors; emendation of the genus *Haloanaerobacter*. Int. J. Syst. Bacteriol. 49 (Pt 1), 103–112.

[12] Jørgensen, B.B. and Des Marais, D.J. (1988) Optical properties of benthic photosynthetic communities: Fiber-optic studies of cyanobacterial mats. Limnol. Oceanogr. 33, 99–113.
[13] Caumette, P., Baulaigue, R. and Matheron, R. (1988) Characterization of *Chromatium salexigens* sp. nov., a halophilic Chromatiaceae isolated from Mediterranean salinas. Syst. Appl. Microbiol. 10, 284–292.
[14] Caumette, P., Baulaigue, R. and Matheron, R. (1991) *Thiocapsa halophila* sp. nov., a new halophilic phototrophic purple sulfur bacterium. Arch. Microbiol. 155, 170–176.
[15] Revsbech, N.P. (1989) An oxygen microelectrode with a guard cathode. Limnol. Oceanogr. 34, 474–478.
[16] Grasshoff, K., Ehrhardt, M. and Kremling, K. (1983) Methods of seawater analysis, Weinheim.
[17] Revsbech, N.P. and Jørgensen, B.B. (1983) Photosynthesis of benthic microflora measured with high spatial resolution by the oxygen microprofile method: Capabilities and limitations of the method. Limnol. Oceanogr. 28, 749–756.
[18] Lassen, C., Ploug, H. and Jørgensen, B.B. (1992) A fibre-optic scalar irradiance microsensor: application for spectral light measurements in sediments. FEMS Microbiol. Ecol. 86, 247–254.
[19] Kühl, M. and Fenchel, T. (2000) Bio-optical characteristics and the vertical distribution of photosynthetic pigments and photosynthesis in an artificial cyanobacterial mat. Microbial Ecol. 40, 94–103.
[20] Castenholz, R.W. (2001) Phylum Bx. Cyanobacteria. Oxygenic Photosynthetic Bacteria, 2nd ed., New York, pp. 473–599.
[21] Nübel, U., Garcia-Pichel, F. and Muyzer, G. (1997) PCR primers to amplify 16S rRNA genes from cyanobacteria. Appl. Environ. Microbiol. 63, 3327–3332.
[22] Schäfer, H. and Muyzer, G. (2001) Denaturing Gradient Gel Electrophoresis in Marine Microbial Ecology. pp. 425–468.
[23] Muyzer, G., Brinkhoff, T., Nübel, U., Santegoeds, C., Schäfer, H. and Wawer, C. (1998) Denaturing gradient gel electrophoresis (DGGE) in microbial ecology. Kluwer, Dordrecht, 1–27.
[24] Wheeler, D.L., Church, D.M., Federhen, S., Lash, A.E., Madden, T.L., Pontius, J.U., Schuler, G.D., Schriml, L.M., Sequeira, E., Tatusova, T.A. and Wagner, L. (2003) Database resources of the National Center for Biotechnology. Nucl. Acids Res. 31, 28–33.
[25] Ludwig, W., Strunk, O., Westram, R., Richter, L., Meier, H., Yadhukumar, A., Buchner, A., Lai, T., Steppi, S., Jobb, G., Forster, W., Brettske, I., Gerber, S., Ginhart, A.W., Gross, O., Grumann, S., Hermann, S., Jost, R., Konig, A., Liss, T., Lussmann, R., May, M., Nonhoff, B., Reichel, B., Strehlow, R., Stamatakis, A., Stuckmann, N., Vilbig, A., Lenke, M., Ludwig, T., Bode, A. and Schleifer, K.-H. (2004) ARB: a software environment for sequence data. Nucl. Acids. Res. 32, 1363–1371.
[26] Lane, D.J. (1991) rRNA Sequencing. pp. 115–175.
[27] Weisburg, W.G., Barns, S.M., Pelletier, D.A. and Lane, D.J. (1991) 16S ribosomal DNA amplification for phylogenetic study. J. Bacteriol. 173, 697–703.
[28] Amann, R., Binder, B., Olson, R., Chisholm, S., Devereux, R. and Stahl, D. (1990) Combination of 16S rRNA-targeted oligonucleotide probes with flow cytometry for analyzing mixed microbial populations. Appl. Environ. Microbiol. 56, 1919–1925.
[29] Achenbach, L.A., Carey, J. and Madigan, M.T. (2001) Photosynthetic and phylogenetic primers for detection of anoxygenic phototrophs in natural environments. Appl. Environ. Microbiol. 67, 2922–2926.
[30] Maidak, B.L., Cole, J.R., Lilburn, T.G., Parker Jr., C.T., Saxman, P.R., Farris, R.J., Garrity, G.M., Olsen, G.J., Schmidt, T.M. and Tiedje, J.M. (2001) The RDP-II (Ribosomal Database Project). Nucl. Acids Res. 29, 173–174.
[31] Gauch, J.H.G. (1982) Multivariate Analysis in Community Ecology, New York, p. 298.
[32] Kovach, W.L. (1999) MVSP – a Multivariate Statistical Package for Windows, ver. 3.1., Wales UK.
[33] Grimalt, J.O. and Albaiges, J. (1990) Characterization of the depositional environments of the Ebro Delta (western Mediterranean) by the study of sedimentary lipid markers. Marine Geol. 95, 207–224.
[34] Volkman, J.K., Johns, R.B., Guillan, F.T., Perry, G.J. and Bavor, H.J. (1980) Microbial lipids of an intertidal sediment-I. Fatty acids and hydrocarbons. Geochim. Cosmochim. Acta 44, 1133–1143.
[35] Grimalt, J.O., de Witt, R., Teixidor, P. and Albaiges, J. (1992) Lipid biogeochemistry of *Phormidium* and *Microcoleus* mats. Org. Geochem. 19, 509–530.
[36] Han, J., McCarthy, E.D., Calvin, M. and Benn, M.H. (1968) Hydrocarbon constituents of the blue-green algae *Nostoc muscorum*, *Anacystis nudulans*, *Phormidium luridum* and *Chlorogloea fritschii*. J. Chem. Soc., 2785–2791.
[37] Paoletti, C., Pushparaj, B., Florenzano, G., Capella, P. and Lercker, G. (1976) Unsaponifiable matter of green and blue-green algal lipids as a factor of biochemical differentiation of their biomasses: II. Terpenic alcohol and sterol fractions. Lipids 11, 266–271.
[38] Blumer, M., Guillard, R.R.L. and Chase, T. (1971) Hydrocarbons of marine phytoplankton. Marine Biol. 8, 183–189.
[39] Nes, W.R. and McKean, M.L. (1977). Biogeochemistry of Steroids and Other Isoprenoids, Baltimore, MD.
[40] Nishimura, M. (1977) Origin of stanols in young lacustrine sediments. Nature 270, 711–712.
[41] Patterson, G.W. (1974) Sterols of some green algae. Comp. Biochem. Physiol. B 47, 453–457.
[42] Ballantine, J.A., Lavis, A. and Morris, R.J. (1979) Sterols of the phytoplankton – effects of illumination and growth stage. Phytochemistry 18, 1459–1466.
[43] Orcutt, D.M. and Paterson, G.W. (1975) Sterol, fatty acid and elemental composition of diatoms grown in chemically defined media. Comp. Biochem. Physiol. B 50, 579–583.
[44] Kates, M., Tremblay, P., Anderson, R. and Volcani, B.E. (1978) Identification of the free and conjugated sterol in a non-photosynthetic diatom, *Nitzschia alba* as 24-methylene cholesterol. Lipids 13, 34–41.
[45] Tornabene, T.G., Langworthy, T.A., Holzer, G. and Oro, J. (1979) Squalenes, phytanes and other isoprenoids as major neutral lipids of methanogenic and thermoacidophilic "archaebacteria". J. Mol. Evolut. 13, 73–83.
[46] Solé, A., Gaju, N. and Esteve, I. (2003) The biomass dynamics of cyanobacteria in an annual cycle determined by confocal laser scanning microscopy. Scanning 25, 1–7.
[47] Solé, A., Gaju, N., Guerrero, R. and Esteve, I. (1998) Confocal laser scanning microscopy of Ebro Delta microbial mats. Microsc. Anal. (Europ. Ed) 29, 13–15.
[48] Abed, R.M., Garcia-Pichel, F. and Hernández-Mariné, M. (2002) Polyphasic characterization of benthic, moderately halophilic, moderately thermophilic cyanobacteria with very thin trichomes and the proposal of *Halomicronema excentricum* gen. nov., sp. nov. Arch. Microbiol. 177, 361–370.
[49] Chuecas, L. and Riley, J.P. (1969) Component fatty acids of the total lipids of some marine phytoplankton. J. Marine Biol. Assoc. UK 49, 97–116.
[50] Benlloch, S., López-López, A., Casamayor, E.O., Ovreas, L., Goddard, V., Daae, F.L., Smerdon, G., Massana, R., Joint, I., Thingstad, F., Pedros-Alio, C. and Rodriguez-Valera, F. (2002) Prokaryotic genetic diversity throughout the salinity gradient of a coastal solar saltern. Environ. Microbiol. 4, 349–360.
[51] Casamayor, E.O., Massana, R., Benlloch, S., Ovreas, L., Diez, B., Goddard, V.J., Gasol, J.M., Joint, I., Rodríguez-Valera, F. and Pedrós-Alió, C. (2002) Changes in archaeal, bacterial and eukaryal assemblages along a salinity gradient by comparison of genetic fingerprinting methods in a multipond solar saltern. Environ. Microbiol. 4, 338–348.

[52] Nübel, U., García-Pichel, F. and Muyzer, G. (2000) The halotolerance and phylogeny of cyanobacteria with tightly coiled trichomes (*Spirulina* Turpin) and the description of *Halospirulina tapeticola* gen. nov., sp. nov. Int. J. Syst. Evol. Microbiol. 50, 1265–1277.
[53] Nübel, U., García-Pichel, F. and Muyzer, G. (1997) PCR primers to amplify 16S rRNA genes from cyanobacteria. Appl. Environ. Microbiol. 63, 3327–3332.
[54] Karsten, U. (1996) Growth and organic osmolytes of geographically different isolates of *Microcoleus chthonoplastes* (cyanobacteria). from benthic microbial mats: Response to salinity change. J. Phycol. 32, 501–506.
[55] Guerrero, R., Urmeneta, J. and Rampone, G. (1993) Distribution of types of microbial mats at the Ebro Delta, Spain. Biosystems 31, 135–144.
[56] Jonkers, H.M., Ludwig, R., DeWit, R., Pringault, O., Muyzer, G., Niemann, H., Finke, N. and De Beer, D. (2003) Structural and functional analysis of a microbial mat ecosystem from a unique permanent hypersaline inland lake: 'La Salada de Chiprana' (NE Spain). FEMS Microbiol. Ecol. 44, 175–189.
[57] Navarrete, A., Urmeneta, J. and Guerrero, R. (2001) Physiological status and community composition of microbial mats by signature lipid biomarkers. pp. 111–116.
[58] Cypionka, H. (2000) Oxygen respiration by *Desulfovibrio* species. Ann. Rev. Microbiol. 54, 827–848.
[59] Cypionka, H., Widdel, F. and Pfennig, N. (1985) Survival of sulfate-reducing bacteria after oxygen stress, and growth in sulfate-free oxygen-sulfide gradients. FEMS Microbiol. Lett. 31, 39–45.
[60] Minz, D., Fishbain, S., Green, S.J., Muyzer, G., Cohen, Y., Rittmann, B.E. and Stahl, D.A. (1999) Unexpected population distribution in a microbial mat community: sulfate-reducing bacteria localized to the highly oxic chemocline in contrast to a eukaryotic preference for anoxia. Appl. Environ. Microbiol. 65, 4659–4665.
[61] Minz, D., Flax, J.L., Green, S.J., Muyzer, G., Cohen, Y., Wagner, M., Rittmann, B.E. and Stahl, D.A. (1999) Diversity of sulfate-reducing bacteria in oxic and anoxic regions of a microbial mat characterized by comparative analysis of dissimilatory sulfite reductase genes. Appl. Environ. Microbiol. 65, 4666–4671.
[62] Wieland, A., Zopfi, J., Benthien, M. and Kühl, M. (2004) Biogeochemistry of an iron-rich hypersaline microbial mat (Camargue, France). Microbial Ecology, in press.
[63] Pierson, B.K. and Parenteau, M.N. (2000) Phototrophs in high iron microbial mats: microstructure of mats in iron-depositing hot springs. FEMS Microbiol. Ecol. 32, 181–196.
[64] Volkman, J.K., Guillan, F.T., Johns, R.B. and Eglinton, G. (1981) Sources of neutral lipids in a temperate intertidal sediment. Geochim. Cosmochim. Acta 45, 1817–1828.
[65] Marlowe, I.T., Brassell, S.C., Eglinton, G. and Green, J.C. (1984) Long chain unsaturated ketones and esters in living algae and marine sediments. Org. Geochem. 6, 135–141.
[66] Eglinton, G. and Hamilton, R.J. (1967) Leaf epicuticular waxes. Science 156, 1322.
[67] Barbe, A., Grimalt, J.O., Pueyo, J.J. and Albaigés, J. (1990) Characterization of model evaporitic environments through the study of lipid components. Org. Geochem. 16, 815–828.
[68] Schouten, S., Hartgers, W.A., Lòpez, J.F., Grimalt, J.O. and SinninghеDamsté, J.S. (2001) A molecular isotopic study of 13C-enriched organic matter in evaporitic deposits: recognition of CO_2-limited ecosystems. Org. Geochem. 32, 277–286.